BRAIN COMMUNICATIONS

5′ValCAC tRNA fragment generated as part of a protective angiogenin response provides prognostic value in amyotrophic lateral sclerosis

Marion C. Hogg,[1,2] Megan Rayner,[1] Sergej Susdalzew,[1] Naser Monsefi,[1] Martin Crivello,[1] Ina Woods,[1] Alexa Resler,[1] Lisle Blackbourn,[1] Paola Fabbrizio,[3] Maria Chiara Trolese,[3] Giovanni Nardo,[3] Caterina Bendotti,[3] Leonard H. van den Berg,[4] Michael A. van Es[4] and Jochen H.M. Prehn[1,2]

Loss-of-function mutations in the ribonuclease angiogenin are associated with amyotrophic lateral sclerosis. Angiogenin has been shown to cleave transfer RNAs during stress to produce 'transfer-derived stress-induced RNAs'. Stress-induced tRNA cleavage is preserved from single-celled organisms to humans indicating it represents part of a highly conserved stress response. However, to date, the role of tRNA cleavage in amyotrophic lateral sclerosis remains to be fully elucidated. To this end, we performed small RNA sequencing on a human astrocytoma cell line to identify the complete repertoire of tRNA fragments generated by angiogenin. We found that only a specific subset of tRNAs is cleaved by angiogenin and identified 5′ValCAC transfer-derived stress-induced RNA to be secreted from neural cells. 5′ValCAC was quantified in spinal cord and serum from SOD1^{G93A} amyotrophic lateral sclerosis mouse models where we found it to be significantly elevated at symptom onset correlating with increased angiogenin expression, imbalanced protein translation initiation factors and slower disease progression. In amyotrophic lateral sclerosis patient serum samples, we found 5′ValCAC to be significantly higher in patients with slow disease progression, and interestingly, we find 5′ValCAC to hold prognostic value for amyotrophic lateral sclerosis patients. Here, we report that angiogenin cleaves a specific subset of tRNAs and provide evidence for 5′ValCAC as a prognostic biomarker in amyotrophic lateral sclerosis. We propose that increased serum 5′ValCAC levels indicate an enhanced angiogenin-mediated stress response within motor neurons that correlates with increased survival. These data suggest that the previously reported beneficial effects of angiogenin in SOD1^{G93A} mice may result from elevated levels of 5′ValCAC transfer RNA fragment.

1 Department of Physiology and Medical Physics, Royal College of Surgeons In Ireland, St. Stephen's Green, Dublin, D02 YN77, Ireland
2 SFI FutureNeuro Research Centre, Royal College of Surgeons In Ireland, St. Stephen's Green, Dublin, D02 YN77, Ireland
3 Laboratory of Molecular Neurobiology, Department of Neuroscience, IRCCS - Mario Negri Institute for Pharmacological Research, Via, La Masa, 19, 20156 Milan, Italy
4 Department of Neurology, Brain Centre Rudolf Magnus, University Medical Centre, University Utrecht, The Netherlands

Correspondence to: Jochen H. M. Prehn, Department of Physiology and Medical Physics, Royal College of Surgeons in Ireland, 123 St. Stephen's Green, Dublin 2, Ireland
E-mail: prehn@rcsi.ie

Keywords: amyotrophic lateral sclerosis; angiogenin; tRNA fragment; tiRNA; biomarker

Received March 30, 2020. Revised July 2, 2020. Accepted June 19, 2020. Advance Access publication August 28, 2020

Abbreviations: ALS = amyotrophic lateral sclerosis; Ang = angiogenin; Arg = arginine; BCA = Bicinchonic Acid; BSA = Bovine serum albumine; CAC = Cytosine Adenine Cytosine; CCA = Cytosine Cytosine Adenine; DAPI = 4′,6-diamidino-2-phenylindole; DIG = Digoxigenin; DMEM = Dulbecco's Modified Eagle's Medium; EDTA = Ethylenediaminetetraacetic acid; EV = extracellular vesicle; FBS = fetal bovine serum; FUS = fused in sarcoma; Gly = glycine; HPRA = Health Products Regulatory Authority; IRES = Internal ribosome entry site; OCT = Optimal cutting temperature compound; PBS = Phosphate-buffered saline; RIPA = Radio immunoprecipitation assay buffer; ROI = Region of interest; miRNA = microRNA; RNase = ribonuclease; SDS-PAGE = Sodium dodecyl sulfate–polyacrylamide gel electrophoresis; SSC = Saline sodium citrate buffer; snRNA = small nuclear RNA; SOD1 = superoxide dismutase 1; TBE = Tris/Borate/EDTA buffer; TG = transgenic; tiRNA = transfer-derived stress-induced RNA; tRNA = transfer RNA; Val = valine; WT = wild type

Graphical Abstract

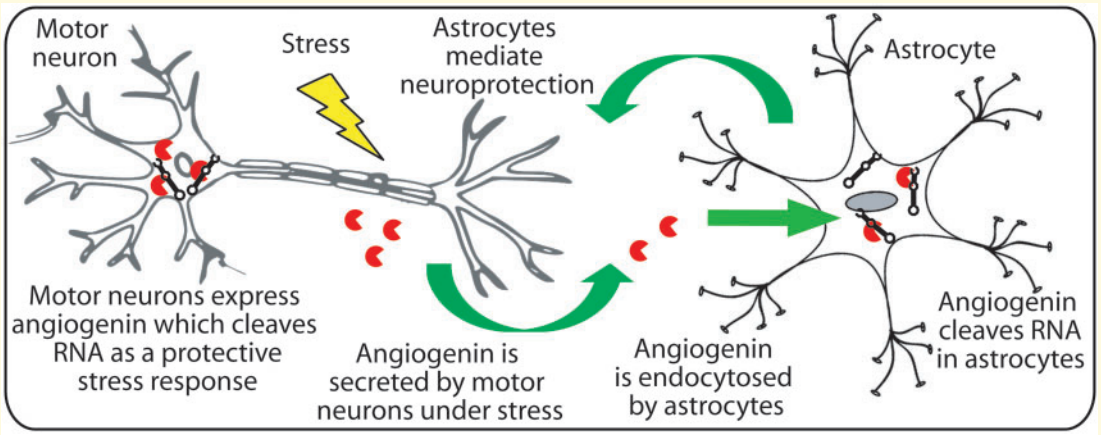

Introduction

Amyotrophic lateral sclerosis (ALS) is a debilitating disease characterized by progressive paralysis, which ultimately leads to death within an average of 3 years from diagnosis (van Es *et al.*, 2017). However, considerable heterogeneity is observed with some patients showing rapid decline and death within 2 years of onset whilst others show a much slower disease progression with survival times extending over 5 years from symptom onset (Pupillo *et al.*, 2014). Therefore, there is a great need to identify prognostic biomarkers for use in ALS.

Angiogenin (Ang) is a ribonuclease (RNase) from the RNase A family, however; it shows significantly lower RNase activity and increased substrate specificity compared to other members of the family (Shapiro *et al.*, 1986). Loss-of-function mutations in the human *ANG* gene were identified in sporadic and familial ALS patients of Irish and Scottish heritage in 2006 (Greenway *et al.*, 2006) and since then mutations have been identified in ALS patients around the world (Aparicio-Erriu and Prehn, 2012). *ANG* variants have also been identified as risk factors for Parkinson's disease (van Es *et al.*, 2011; van Es *et al.*, 2014), and more recently a non-sense mutation was identified in a patient with Alzheimer's disease (Gagliardi *et al.*, 2018), indicating Ang may have a more widespread role in neuronal protection. Ang is expressed in many cell types, including motor neurons and endothelial cells (Greenway *et al.*, 2006; Wu *et al.*, 2007), and production and secretion of Ang are upregulated in response to stresses such as hypoxia or trophic factor withdrawal (Sebastia *et al.*, 2009; Skorupa *et al.*, 2012). Our group and others have shown that Ang protects primary neurons against metabolic and toxic challenges *in vitro* (Fu *et al.*, 2009; Kieran *et al.*, 2008; Steidinger *et al.*, 2011; Skorupa *et al.*, 2012; Ivanov *et al.*, 2014). Furthermore, systemic administration of recombinant human Ang protein prevented motor neuron death and increased lifespan in the $SOD1^{G93A}$ mouse model of ALS (Kieran *et al.*, 2008; Crivello *et al.*, 2018). Interestingly, transcriptomic analysis of fast and slow progressing mice expressing the same $SOD1^{G93A}$ transgene on different genetic backgrounds revealed that Ang expression in motor neurons was higher in slow-progressing compared to fast-progressing mice (Nardo *et al.*, 2013), again suggesting that Ang elicits protective stress responses. Subsequent studies indicated that secreted or systemically administered Ang is endocytosed predominantly by astrocytes *in vitro* and *in vivo* (Skorupa *et al.*, 2012; Crivello *et al.*, 2018).

Ang has been shown to cleave transfer RNAs during stress to produce 'transfer-derived stress-induced RNAs' ('tiRNAs') (Yamasaki et al., 2009; Saikia *et al.*, 2012; Honda and Kirino, 2016). Stress-induced tRNA cleavage

is preserved from single-celled organisms to humans indicating it represents part of a highly conserved stress response (Lee and Collins, 2005). Using small RNA sequencing and custom bioinformatic analysis, we found that a specific subset of tRNAs was robustly cleaved by Ang within the anticodon loop, from which only one half was retained. We found that 5′ValCAC was elevated at disease onset in the spinal cord from slow-progressing $SOD1^{G93A}$ transgenic (TG) mice, which correlated with increased Ang levels and differential expression of protein translation initiation factors. We validated these results in a second preclinical ALS mouse, the fused in sarcoma (FUS) (1-359) model. We describe serum 5′ValCAC tRNA fragment as a novel prognostic biomarker in ALS, which results from a beneficial Ang-mediated neuroprotective stress response in motor neurons.

Materials and methods

Cell culture

MZ-294 cells (RRID: CVCL_M410) were originally isolated from a primary glioblastoma (Hetschko *et al.*, 2008) and maintained at 37°C/5% CO_2 in DMEM media (Lonza) supplemented with 10% FBS (Sigma), 2 mM L-Glutamine (Sigma), 100 U/ml Penicillin and 0.1 mg/ml Streptomycin (P/S: Sigma). Astrocyte lineage was confirmed by S100β expression (Raponi *et al.*, 2007). Cells were treated with recombinant human angiogenin (rhAng: R&D Systems, #265-AN/CF) in serum-free Neurobasal media (ThermoFisher Scientific).

SH-SY5Y human neuroblastoma cells (RRID: CVCL_0019) were obtained from the ATCC and maintained in DMEM/F12 media (ThermoFisher Scientific) with additions as above. SH-SY5Y cells stably overexpressing Ang were generated by transfection of pcDNA3.1-*ANG* WT or mutant plasmids with Metafectene (Biontex Laboratories GmbH), and selection performed with neomycin (G418, Sigma).

Cell lines were confirmed as free from mycoplasma infection.

Nuclear and cytoplasmic fractionation

Nuclear and cytoplasmic fractionation was performed as described (Suzuki *et al.*, 2010). Briefly, cells were washed in ice-cold PBS, scraped into 1 ml PBS and pelleted by centrifugation for 10 s at 4°C with 16 000 × g. The supernatant was discarded, and the cell pellet resuspended in 100 µl PBS with 0.1% NP-40 with protease inhibitors (Sigma). The cell pellet was triturated five times with a P1000 pipette tip and the sample was centrifuged for 10 s at 4°C with 16 000 × g. The supernatant was collected as a cytoplasmic fraction, and the pellet was washed twice by resuspending in PBS with 0.1% NP-40. The supernatant was discarded, and the pellet (nuclear fraction) resuspended in 30 µl RIPA buffer (50 mM Tris-HCl, pH 7.5, 150 mM NaCl, 1 mM EDTA, 1% Triton X-100, 0.25% sodium deoxycholate) with protease inhibitors (Sigma). Nuclear and cytoplasmic fractions for protein analysis were triturated and incubated on ice for 15 min before a final centrifugation step for 1 min at 4°C and 10 000 × g. Nuclear and cytoplasmic fractions for RNA analysis were extracted with Trizol reagent as described.

Extracellular vesicle purification

Extracellular vesicles (EVs) were purified from conditioned media [CM: 24 h, serum-free neurobasal media (Sigma)] following a described protocol (Chakrabortty *et al.*, 2015). Briefly, CM was collected and centrifuged at 2000 × g for 10 min, then passed through a 0.22 µm syringe filter. EVs were precipitated from 10 ml CM by addition of 2 ml ExoQuick TC solution (System Biosciences). Samples were incubated overnight at 4°C. EVs were pelleted by centrifugation at 1500 × g for 30 min at 4°C, the supernatant was discarded. EVs were resuspended in 110 µl PBS with a 10 µl sample used for NanoSight NTA particle analysis and 100 µl used for RNA extraction. Expression of exosomal markers was confirmed by western blotting, where EVs from 10 ml CM were resuspended in 25 µl RIPA buffer, and analysed as described. Antibodies used were Rabbit anti-Alix (Bethyl Laboratories, A302-938A, RRID: AB_10681518) and Rabbit anti-Flotillin 1 (Abcam, ab RRID: AB_941621).

RNA extraction and analysis

Total RNA was extracted from cells using Trizol reagent and protocol (ThermoFisher Scientific). Briefly, a 10 cm dish was collected in 1 ml Trizol reagent and incubated for 5 min at room temperature. A 200 µl of chloroform was added, and samples were shaken for 15 s. Samples were centrifuged at 12 000 × g for 15 min at 4°C. The aqueous phase was removed to a new tube, and an equal volume of isopropanol was added. Samples were incubated overnight at −20°C. Samples were centrifuged at 12 000 × g for 15 min at 4°C. The pellet was washed with 75% ethanol and air dried before resuspension in water supplemented with RNaseOUT RNase inhibitor (ThermoFisher Scientific). RNA was extracted from mouse tissue using the Qiagen miRNeasy kit (Qiagen) and quantified by Nanodrop. RNA was purified from serum or conditioned media using the Qiagen serum/plasma miRNeasy kit (Qiagen). 3.5 µl of *Caenorhabditis elegans* microRNA (miRNA)-39 spike-in (at 1.6 × 10^8 copies/µl) was added during purification according to the manufacturer's instructions (Qiagen). RNA was eluted in 20 µl water containing 1 µl RNaseOUT RNase inhibitor.

Small RNA levels were quantified by Fragment Analyser (Advanced Analytical).

Small RNA sequencing and analysis

Small RNA sequencing was performed on total RNA <100 nt extracted from three biological replicates of MZ-294 cells treated with rhAng or vehicle by Eurofins MWG (error ~25%; Supplementary Fig. 1). Adaptor sequences were trimmed using Trim Galore with 10 bp adaptor overlap and 10% errors (using cutadapt -O 10 -e 0.1 parameters). Reads with quality score <20 or length <15 bp were filtered out. A tRNA database was built from the tRNA genome downloaded from GtRNAdb (gtrnadb.ucsc.edu). Intron locations were added for 32 tRNAs. Tophat (v 2.0.14) and Bowtie (v 2.2.5.0) were used for alignments. Alignments were done in three stages:

(1) Filtered reads were aligned to custom tRNA database with 1 hit allowed per read (-x 1 parameter) and mapped to tRNAs.
(2) Unmapped reads from step 1 were aligned to the human genome (GRCh37/hg19) with 1 hit allowed per read (-x 1 parameter) and mapped to the sno/miRNA transcriptome.
(3) Unmapped reads from step 2 were aligned to the human genome with 60 hits allowed per read, and reads were mapped to RefSeq transcriptome.

Aligned reads were counted and differential expression analysis was performed using DESeq2, including adjustment of *P*-values to correct for multiple testing (Love *et al.*, 2014). RNA secondary structures were predicted using the Vienna RNAfold program (Lorenz *et al.*, 2011).

RNA gel and northern blotting

RNA gels were performed as described (Skorupa *et al.*, 2012). Briefly, 15 µg total RNA isolated with Trizol reagent, and the protocol was diluted in formamide loading buffer and denatured at 90°C for 5 min before loading onto a 15% TBE-Urea PAGE gel. Gels were electrophoresed at 200 V for 95 min at 4°C, stained with SYBR Gold (ThermoFisher Scientific), and imaged on an LAS 4000 Reader (Fujifilm). Northern blotting was performed as described (Kim *et al.*, 2010). Briefly, following RNA gel electrophoresis, RNA was transferred to a Hybond+ nitrocellulose membrane (GE Lifesciences) at 10 V for 60 min at 4°C. RNA was UV-cross-linked in a Stratalinker (1200 mJ/cm^2). Membranes were blocked in ultraHyb Oligo (ThermoFisher Scientific) for 30 min at 37°C. Dual digoxigenin-labelled DNA probes were added to the blocking solution (final concentration 1 nM) and incubated overnight at 37°C. Membranes were washed twice with low-stringency wash buffer (2× SSC, 0.1% SDS) and twice with high-stringency wash buffer (0.1× SSC, 0.1% SDS) at 37°C, then 2× SSC at room temperature. Membranes were processed using the DIG wash and block set according to instructions (Roche). CPD-Star Development Reagent (Roche) was added and images were acquired using a LAS 4000 Reader (Fujifilm). Dual digoxigenin-labelled probes are listed in Supplementary Table 2.

qPCR

Custom small RNA Taqman assays (ThermoFisher Scientific) were designed to 5′ValCAC tiRNA fragment (5′-GUUUCCGUAGUGUAGUGGUUAUCACGUUCGCCUC-3′) and quantification performed on StepOnePlus or Quantstudio 5 PCR machines (ThermoFisher Scientific). Assay I.D. available on request. Mouse tiRNA levels were normalized to U6 snRNA, and human tiRNA levels were normalized to *C. elegans* miRNA-39 spike-in, using the 2^{-DDCt} method (Livak and Schmittgen, 2001). A 2 µl RNA per reverse transcription was performed according to the Taqman small RNA Assay protocol (ThermoFisher). A 1 µl reverse transcription per qPCR reaction, and qPCRs were performed in triplicate. Ang expression analysis was performed using Quantitect SYBR green PCR kit (Qiagen) using primers from Fu *et al.* (2009).

Immunocytochemistry and immunohistochemistry

Immunocytochemistry was performed on MZ-294 cells treated with rhANG or vehicle using goat anti-human Ang (1/100, PC317L, Calbiochem, RRID: AB_213593) and mouse anti-tubulin (1/500, T6199, Sigma, RRID: AB_477583). Cells grown on coverslips were treated with rhAng or vehicle and fixed in 4% paraformaldehyde for 15 min. Cells were permeabilized by 10 min incubation in 95% ethanol: 5% glacial acetic acid. Coverslips were blocked in 5% BSA in PBS with 0.1% Triton X-100. Primary antibodies were incubated overnight at 4°C. Fluorescent Alexa-conjugated secondary antibodies were used (1/500, Molecular Probes) for 2 h and coverslips mounted in Prolong Gold (Invitrogen). Images were captured on a Zeiss LSM 710 confocal microscope.

Anaesthetized mice were perfused transcardially with 4% paraformaldehyde and spinal cord dissected, post-fixed in 4% paraformaldehyde overnight at 4°C, preserved in 30% sucrose and then included in OCT compound. Immunohistochemical analyses were done on free-floating spinal cord cryosections (30 μm), after mounting on glass slides (Walderlmar Knittle) with 1:1 0.1 M PBS: glycerol, samples were analysed under an Olympus Fluoview Laser scanning confocal microscope (Olympus BX61 light microscope). Z-stacked composites were generated and used for image analysis. The primary antibodies used: mouse anti eIF4e (1/200, sc-9976, Santa Cruz Biotechnology, RRID: AB_627502) and rabbit anti eIF4eBP1 (1/500, SAB4300475, Sigma-Aldrich, RRID:

AB_10634621). Alexa- 488 and 647 secondary antibodies (Invitrogen) were used at 1:500. The intensity of fluorescence was calculated with Fiji (Image J, U. S. National Institutes of Health, Bethesda, MD, USA) on a single cell by making an ROI on the cytosol of each MN with a diameter $>$ 400 μm^2 and measuring the Integrated Density following background subtraction. ~3–5 MNs $>$ 400 μm^2 from at least three serial L3–L4 slices were evaluated.

Western blotting

Lysates were collected in RIPA buffer (50 mM Tris-HCl, pH 7.5, 150 mM NaCl, 1 mM EDTA, 1% Triton X-100, 0.25% sodium deoxycholate) with protease inhibitor (Sigma). Total protein was quantified using a macro BCA assay (ThermoFisher Scientific) and denatured for 10 min at 90°C in 1× laemmli buffer. Proteins were separated on a 12% SDS-PAGE gel and transferred to a nitrocellulose membrane. Membranes were incubated overnight in antibodies: goat anti-human Ang (1/500, AB-265-AN, R & D Systems, RRID: AB_354325) and mouse anti-actin (1/1000, A5441, Sigma, RRID: AB_476744). Membranes incubated for 2 h in HRP-conjugated secondary antibodies. ECL reagent was added (Immobilon, Merck), and images were taken on a LAS 4000 Reader (Fujifilm).

ALS mouse models

FUS (1-359) mice (Shelkovnikova *et al.*, 2013) were kindly donated by Professor Vladimir Buchman (School of Biosciences, Cardiff University, Cardiff, CF10 3AX, UK), embryos were re-derived in The Institute of Molecular Genetics ASCR, Prague, Czech Republic, and the colony maintained at RCSI. Ethical approval for the study was granted by the RCSI Research Ethics Committee (REC1122), and a licence was obtained from the HPRA (AE19127/P004). After weaning on post-natal day 21, pups from litters of the same generation and gender were housed in groups (3–5 per cage). $N = 6$–8 mice of both sexes were used in this study.

TG $SOD1^{G93A}$ mice of C57BL/6JOlaHsd (C57-TG) or 129SvHsd (129Sv-TG) genetic background and non- TG littermates (C57-WT and 129Sv-WT) derived from the B6SJL-TgNSOD-1-$SOD1^{G93A}$-1Gur line (Jackson Laboratories) expressing 20 copies of human $SOD1^{G93A}$ transgene were maintained at the Mario Negri Institute animal facility. Procedures involving animals were conducted according to the Mario Negri institutional guidelines. The Statement of Compliance (Assurance) with the Public Health Service (PHS) Policy on Human Care and Use of Laboratory Animals has been recently reviewed (9/9/2014) and will expire on 30 September 2019 (Animal Welfare Assurance #A5023-01). Symptom onset was determined by the first sign of impaired paw grip strength and decline in body weight. $N = 8$ female mice at symptom onset were used in this study. Mice were maintained at 22 ± 2°C with a relative humidity 55 ± 10% and a 12 h light/dark cycle with food and water supplied *ad libitum*.

Tissue and serum collection

Animals were terminally anaesthetized with Dolethal, and after the absence of reflexes was confirmed, blood was collected. Serum was separated by centrifugation at 1000 × g for 10 min at 4°C. Mice were transcardially perfused with PBS, and the spinal cord was dissected and frozen.

Patient samples

Serum samples were from the Prospective ALS study Netherlands (PAN), which is a large ongoing epidemiological study on environmental and genetic risk factors for ALS (Huisman *et al.*, 2011). Male and female ALS patients fulfilled the criteria for suspected, possible, probable or definite ALS according to the 1994 El Escorial criteria (Brooks, 1994). In the PAN study, practitioners are asked to recruit a matched for age, sex and ethnicity control individual for each ALS case. Samples included in this study came from participants enrolled in the PAN study in 2013 and 2014. DNA samples from the individuals in the discovery cohort were screened for mutations in *C9orf72*, *TARDBP*, *SOD1*, *FUS* and *ANG* by whole genome sequencing (Dolzhenko *et al.*, 2017; van Rheenen *et al.*, 2016). All participants provided informed consent according to the Declaration of Helsinki. Ethical approval for this study was obtained from the Institutional Review Board of UMC Utrecht. Blood was centrifuged at 1000 × g and serum collected and stored at −80°C. Serum was checked for haemolysis on the Nanodrop using a protocol adapted from Appierto *et al.* (2014).

Statistical analysis

Statistical analysis was performed in Graphpad Prism, SPSS or R version 3.4.3. Data are fold change tiRNA levels in TG compared to wild type (WT) mice, or ALS patients compared to controls. Student's *t*-tests and ANOVA were used to determine whether mean tiRNA levels differed between WT and TG groups and groups of more than two, respectively. Tukey's honest significant difference test was used to assess differences between specific group means. In patient samples, tiRNA levels were tested using a Kruskal–Wallis test with *post hoc* Dunn's test. As exploratory analyses, Poisson regression with robust standard errors was used to compute relative risk estimates and 95% confidence intervals to examine whether each continuous linear tiRNA was independently associated with the risk of slow versus fast ALS progression. Analyses were adjusted for continuous linear age at sample collection and binary gender. Statistical significance was determined from Wald *P*-values computed using robust standard errors. Receiver operating characteristics curve analysis was performed in SPSS and Youdens J statistic was used to identify the maximal potential effectiveness of the biomarker.

Data availability

Raw RNA sequencing reads are deposited in the NCBI Sequence Read Archive (BioProject PRJNA507979).

Results

Small RNA sequencing to identify substrates of Ang

Motor neurons express Ang and during stress conditions expression is increased and Ang is secreted (Greenway *et al.*, 2006; Wu *et al.*, 2007). We have shown Ang is endocytosed by astrocytes where it cleaves RNA and mediates neuroprotection in paracrine (Skorupa *et al.*, 2012). The human glial-derived cell line MZ-294 was used to characterize Ang substrates, as these cells do not express detectable levels of Ang and efficiently endocytose Ang from media (Fig. 1A). Exogenous recombinant human Ang (rhAng) added for 3 h is predominantly located in the cytoplasm (Fig. 1B) and induces RNA cleavage in a dose-dependent manner (Fig. 1C). To determine the composition of RNA fragments, we isolated total RNA from Ang-treated (500 ng/ml in PBS with 1% BSA; 3 h; R&D Systems) and vehicle-treated cells (PBS with 1% BSA; 3 h) and performed small RNA sequencing (<100 nt, Supplementary Fig. 1). We developed a custom analysis pipeline using a tRNA library generated from the human tRNA genome at GtRNAdb (gtrnadb.ucsc.edu; Chan and Lowe, 2009). The GtRNAdb is a publicly available catalogue of predicted tRNA gene sequences from over 700 different species with direct links to the UCSC genome browser to allow users to view tRNAs in their genomic context. To account for the post-transcriptional addition of CCA-tails to tRNAs, 'CCA' was added to the 3′ end of each tRNA. Reads aligning to tRNAs were pooled by isoacceptor type, differential gene expression was performed, and read coverages plotted to determine the Ang cleavage profile. Read distribution (listed in Supplementary Table 1) indicated a similar proportion of reads aligned in Ang and vehicle-treated cells, including tRNA aligned reads (4% Ang and 3.6% vehicle).

Specific tRNAs are cleaved by Ang

Read profiles indicated a small but highly significantly altered subset of tRNAs were robustly cleaved by Ang (Table 1). Full-length tRNAs were not detected in this analysis due to the high frequency of modified bases, which inhibits the progression of polymerases. When we limited the analysis to significantly altered tRNAs with an adjusted P-value < 0.05, we identified 10 tRNAs, 9 of which showed profiles indicative of cleavage by Ang, suggesting tRNA cleavage is a highly specific process. Specific aminoacyl groups were favoured by Ang (e.g. arginine and valine) whilst others remained intact. In most cases, reads were detected aligning to either the 5′ or 3′ end of the tRNA, which appeared to be determined by aminoacyl group as 3′ fragments were only identified from arginine tRNAs. Aligned reads for Valine CAC genes are shown (Fig. 1D) with chromosomal location and gene sequence below (Fig. 1E). A dramatically different profile is seen in Ang-treated cells where many short RNA fragments aligned to the 5′ end of Valine CAC which are absent in vehicle-treated cells. Mapping the cleavage site onto the secondary structure indicated Ang cleavage predominantly occurred within the anticodon loop (Fig. 1F, mature full-length Valine CAC secondary structure; Fig. 1G predicted 5′Valine CAC tiRNA secondary structure). Read coverage plots and predicted secondary structures for tRNAs listed in Table 1 are provided in Supplementary Figs 2–10. The tRNA fragments are predicted to form stable hairpin structures (Supplementary Figs 11 and 12) and interestingly, the preserved fragments have higher predicted minimum free energy than the undetected fragments (Supplementary Fig. 13).

Validation of tRNA fragment accumulation in response to Ang

Northern blotting was used to validate tRNA cleavage by Ang (Fig. 2A) with probes that recognize 5′ValCAC, 3′ArgTCG and 5′GlyGCC. Probes recognizing 3′3′ValCAC and 5′ArgTCG fragments showed these are barely detectable indicating they undergo rapid degradation and validating the RNA seq results. The 5S ribosomal RNA band from the RNA gel is included to show equal loading of total RNA. Nuclear and cytoplasmic fractionation revealed cleavage occurs within the cytoplasm (Fig. 2B), a western blot confirming fractionation is shown (Fig. 2D). The proportion of tRNA that is cleaved by Ang relative to full-length tRNA Valine CAC is low (conservatively estimated at 5-fold more full-length compared to fragment, see Supplementary Fig. 14), suggesting there would be no loss-of-function of full-length tRNAs associated with tRNA cleavage. Custom small RNA Taqman assays were designed to recognize specific tiRNA fragments 5′ValCAC, 3′ArgTCG and 5′GlyGCC. Custom synthetic tiRNA mimics were synthesized for 5′ValCAC, 3′ArgTCG and 5′GlyGCC (IDT, USA) and used as a template for qPCR. Synthetic tiRNAs amplified linearly over a range of four orders of magnitude (Fig. 2C) indicating the Taqman assays were robust. The Taqman assays displayed a dose–response to increasing Ang levels in both human astrocytoma and mouse primary astrocytes (Fig. 2E and F) although the response to Ang was muted in primary mouse astrocytes.

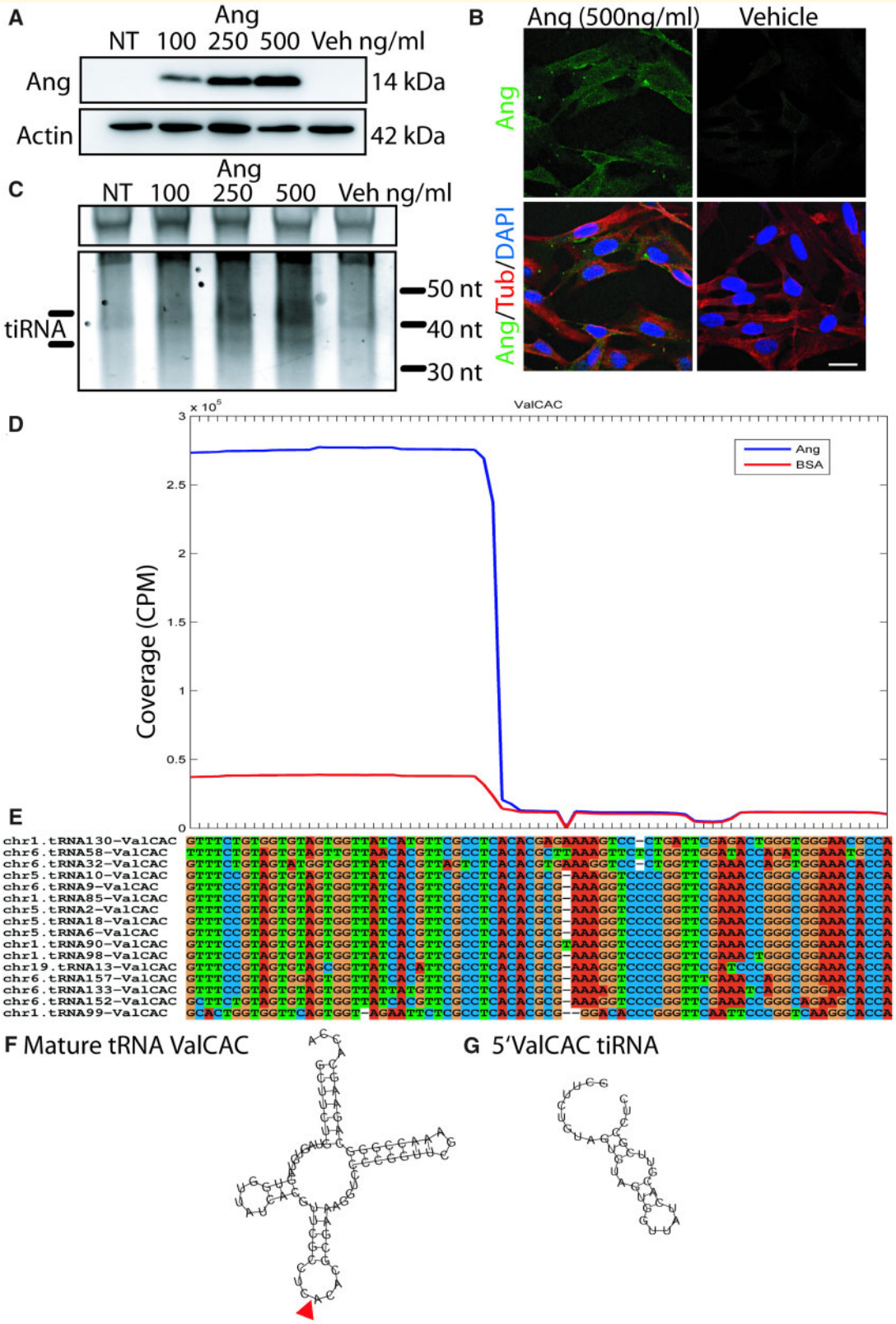

Figure 1 Small RNA sequencing to identify substrates of Ang. (**A**) Western blot showing rhAng in serum-free media is endocytosed by glial-derived MZ-294 cells in a dose-dependent manner (doses are 100, 250, and 500 ng/ml). Untreated (NT) or vehicle-treated (Veh) MZ-294 cells do not contain detectable levels of Ang. Uncropped blots are available in Supplementary material. (**B**) Immunocytochemistry of Ang and vehicle-treated MZ-294 showing that Ang (Green) is clearly detectable in the cytoplasm highlighted here with tubulin (Red) following 3 h treatment (500 ng/ml). Nuclei are stained with DAPI, scale bar = 25 μm. (**C**) SYBR Gold stained TBE-Urea RNA gel showing RNA fragmentation induced by Ang in a dose-dependent manner. tiRNAs of approximately 34 and 43 nt are indicated, a ribosomal RNA band is shown as a loading

(continued)

Table 1 Table displaying the significantly altered tRNAs.

tRNA	Mean of normalized counts	Log_2 fold change: Ang versus BSA	Adjusted *P*-value	5′ or 3′
ValCAC	53 744	2.35	1.87E−43	5′
ArgCCG	13 220	2.10	1.48E−07	3′
GlyGCC	24 549	1.38	1.48E−07	5′
ArgTCG	10 369	2.22	4.59E−07	3′
LysCTT	66 611	1.03	6.04E−05	5′
ArgTCT	7437	1.57	0.0010	3′
PseudoCAC	15	1.74	0.0025	5′
ArgCCT	17 098	0.58	0.0056	3′
SerAGA	6716	−0.53	0.0099	Both*
ValAAC	17 162	0.74	0.0146	5′

tRNAs ranked by adjusted *P*-values, with raw *P*-values also listed. Mean of the normalized read counts for all samples are shown indicating the abundance of the tRNA fragments (Pseudo CAC reads were negligible), and a summary of whether 5′ or 3′ tiRNA was detected, * fragments from both 5′ and 3′ ends of SerAGA were detected, see supplementary data for the cleavage profiles of all listed tRNAs.

tiRNA secretion from neuronal cells is altered by ALS-associated *ANG* mutations

As endogenous Ang is expressed in motor neurons (Greenway *et al.*, 2006), we explored whether tRNA cleavage also occurs in neuronal cells. Further, as miRNAs are actively secreted from cells in argonaute-bound complexes or protected within exosomes (Chen *et al.*, 2012), and tiRNAs have been found within synaptic vesicles (Li *et al.*, 2015) we sought to determine whether tiRNAs are secreted from neuronal cells, and could be detected in exosomes. We used human neuroblastoma SH-SY5Y cell lines that stably overexpress WT *ANG*, or ALS-associated mutants K40I and R31K. The K40I mutation renders Ang catalytically inactive while the R31K mutation is reported to inhibit nuclear translocation (Thiyagarajan *et al.*, 2012). qPCR and western blotting confirmed Ang over-expression compared to the control, which stably expresses the pcDNA3.1 plasmid (Fig. 3A and B, pcDNA). The K40I mutant was consistently produced at lower levels (in multiple clones generated) than WT Ang or R31K mutant indicating this mutation may affect the stability of *ANG* mRNA (data not shown). Cells were incubated for 24 h in serum-free media and conditioned media (CM) collected. Quantification of 5′ValCAC indicated 5′ValCAC was secreted at elevated levels from cells overexpressing WT *ANG* and R31K mutant *ANG* compared to the pcDNA control and the K40I mutant (Fig. 3C). The R31K mutation is located within the nuclear localization signal of Ang, and we see increased 5′ValCAC secreted indicating the R31K mutation may interact with cytoplasmic factors involved in the secretion pathway. We explored the mechanism of tiRNA secretion by precipitating EVs from CM. There was no significant difference in EV numbers purified from cells stably overexpressing WT or mutant *ANG* (Fig. 3D). Exosomal markers were present on purified EVs as shown by western blotting with Alix and Flotillin 1 antibodies (Fig. 3E). We found that the fraction of 5′ValCAC in EVs was not significantly different between the cell lines, with ∼2–4% total secreted 5′ValCAC found in EVs (Fig. 3F). This suggests that the un-encapsulated fraction of 5′ValCAC is dynamically regulated while basal levels of 5′ValCAC are secreted in EVs.

5′ValCAC levels indicate disease progression in mouse models of ALS

As tiRNA production is linked to protective stress signalling (Fu *et al.*, 2009; Emara *et al.*, 2010; Saikia *et al.*, 2012; Saikia *et al.*, 2014), we investigated 5′ValCAC levels in slow versus fast-progressing $SOD1^{G93A}$ mice bred on two distinct genetic backgrounds (C57Bl/6JOlaHsd and 129 Sv), which display differences in disease progression and lifespan (Nardo *et al.*, 2013). $SOD1^{G93A}$ TG mice on the 129Sv background show symptom onset at 14 weeks whereas TG mice on the C57/Ola background show delayed symptom onset at 18 weeks (Fig. 4A). This difference could not be explained by differences in $SOD1^{G93A}$ transgene copy number or levels of mutant SOD1 protein (Nardo *et al.*, 2013). Interestingly, Nardo

Figure 1 Continued
control. (**D**) Pooled read coverage (counts per million) of reads aligned to Valine CAC genes, with genomic location and gene sequences shown in (**E**). A clear cleavage profile is present in Ang -treated samples where the 5′ValCAC fragment is retained while the 3′ fragment is absent. Full-length tRNA reads were not detected due to the highly modified nature of tRNAs, which inhibits the progression of polymerases. (**F**) Mature tRNA Valine CAC secondary structure with the Ang cleavage site in the anticodon loop indicated (red triangle). (**G**) Predicted secondary structure of the 5′ValCAC tiRNA fragment.

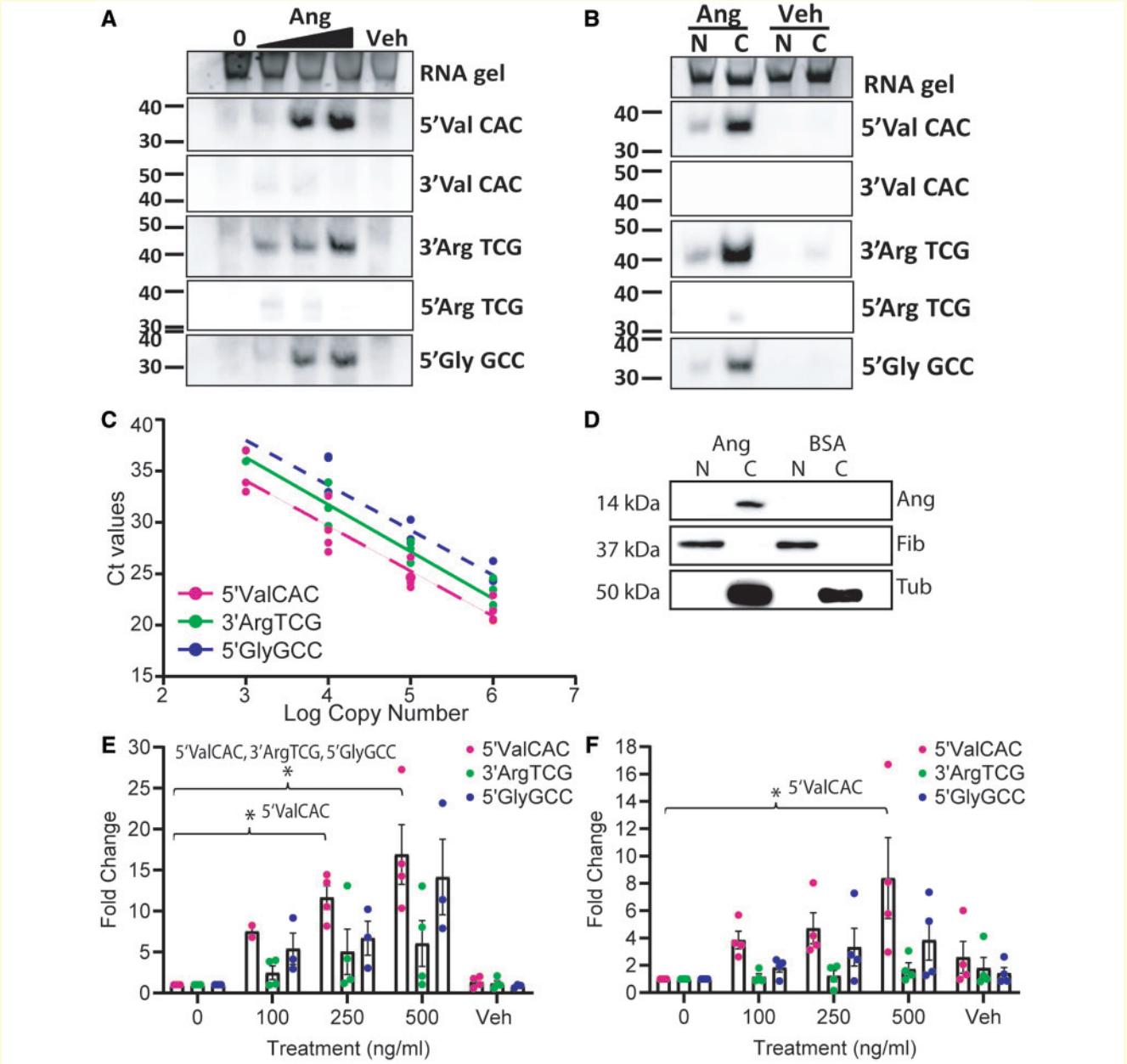

Figure 2 Specific tRNA fragments accumulate in Ang -treated astrocytes. (**A**) tiRNA production was validated using northern blotting with dual DIG labelled probes specific for either the 5′ or 3′ end of the tRNA, which shows the 5′ValCAC fragment increases with higher doses of Ang whereas the 3′ ValCAC fragment is barely detectable in all samples. Similarly, the 5′GlyGCC and 3′ArgTCG tiRNAs increase in a dose-dependent manner whereas the 5′ ArgTCG cannot be detected at all. 5S ribosomal RNA on the RNA gel is shown to demonstrate similar levels of RNA were loaded in each lane. (**B**) Nuclear and cytoplasmic fractionation was performed to determine where Ang cleavage occurs which revealed the tiRNA fragments are generated in the cytoplasm. Uncropped blots are available in Supplementary material. (**C**) Custom Taqman assays were designed to recognize 5′ValCAC, 3′ ArgTCG and 5′ GlyGCC tiRNAs, and standard curves were generated using synthetic tiRNAs (Integrated DNA technologies) which showed the Custom Taqman assays are linear log over a 4-fold dilution series (R2 values: 5′ValCAC = 0.99, 3′ArgTCG = 0.99, 5′GlyGCC = 0.97), $n = 4$ independent experiments, individual data points are shown. (**D**) Nuclear and cytoplasmic fractionation was confirmed by western blotting with nuclear (Fibrillarin) and cytoplasmic (Tubulin) antibodies. Taqman assays were validated in (**E**) MZ-294 human astrocytoma cells and (**F**) Primary mouse astrocytes treated with increasing amounts of rhAng. $N = 4$ independent experiments, with individual data points and mean ± SEM shown. * indicates $P < 0.05$, one-way ANOVA *post hoc* Dunnett's compared to 0 Ang. In (**E**), all three assays show a significant difference between 0 and 500 ng/ml Ang, and 5′ValCAC assay shows a significant difference between 0 and 250 ng/ml Ang. In (**F**), 5′ValCAC assay shows a significant difference between 0 and 500 ng/ml Ang.

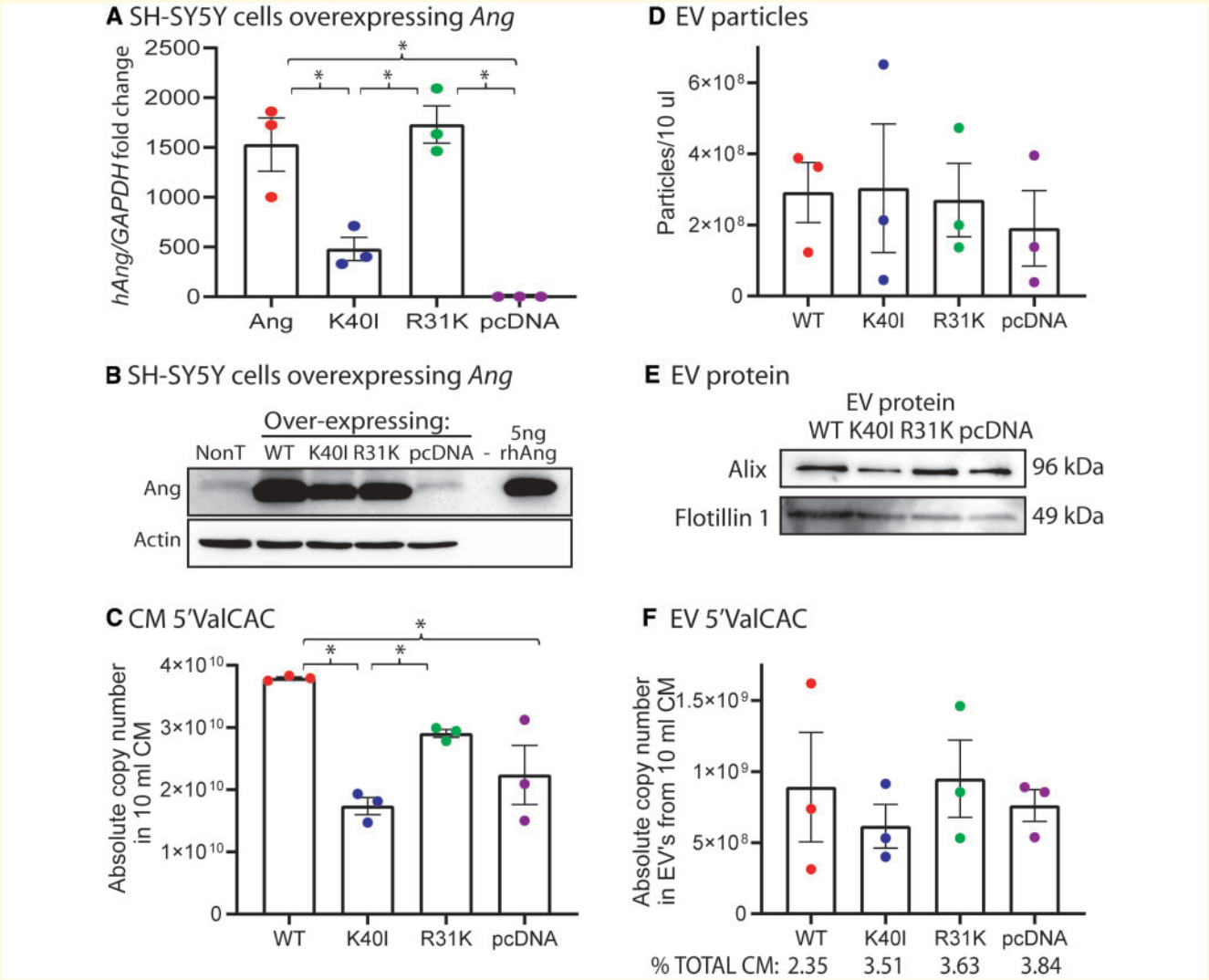

Figure 3 tiRNAs are secreted from neuronally derived cells. SH-SY5Y human neuroblastoma cells stably over-expressing WT human *ANG* (Ang) or ALS-associated mutants (K40I, R31K), or the empty vector alone (pcDNA) were generated, and Ang levels were quantified by (**A**) qPCR and (**B**) western blot. Recombinant human Ang (5 ng) was loaded as a control. The K40I mutant consistently displayed reduced expression indicating this mutation may alter the stability of the *ANG* mRNA. Uncropped blots are available in Supplementary material. (**C**) Absolute levels of 5′ValCAC tiRNA were examined in conditioned media (CM) using a custom Taqman assay revealing levels were increased in WT and R31K expressing cells, whereas no increase was detected in CM from cells expressing the catalytically inactive K40I mutant, or the empty vector. $N = 3$ independent experiments each, data represent mean ± SEM with individual data points shown. (**E**) Precipitation of EVs from all cell lines showed no significant difference in the number of particles purified from stable cell lines expressing WT or mutant *ANG*. (**F**) EVs expressed Alix and Flotillin 1 indicating exosomes were present. Uncropped blots are available in Supplementary material. (**G**) 5′ValCAC was present in EVs but levels were low across all cell lines analysed, compared to the amount in total CM (indicated as percent of total below the graph). The majority of the extracellular 5′ValCAC is un-encapsulated, and this appears to be dynamically regulated by Ang as significantly higher levels were found in WT and R31K mutant overexpressing cell lines compared to K40I or pcDNA control.

et al. (2013) found significantly increased Ang expression in the C57/Ola strain at symptom onset. Therefore, we examined Ang expression and 5′ValCAC levels in lumbar spinal cord RNA collected at symptom onset in these $SOD1^{G93A}$ mice. Initially, we confirmed *mAng1* levels were significantly elevated in the slow-progressing TG mice compared to WT mice on the C57/Ola background, and also compared to fast-progressing 129 Sv WT and TG mice (Fig. 4B). We then found that 5′ValCAC levels were significantly higher in the spinal cord from the slow TG mice compared to the fast TG and WT mice (Fig. 4C), suggesting that 5′ValCAC may serve as a biomarker of disease progression in ALS.

tiRNAs have been shown to inhibit protein translation in several recent studies (Ivanov *et al.*, 2011; Goncalves *et al.*, 2016; Fricker *et al.*, 2019). The protein translation initiation factor eIF4e plays a crucial role in recruiting eIF4G and subsequently the ribosomal subunits to the 5′m7G mRNA cap structure.

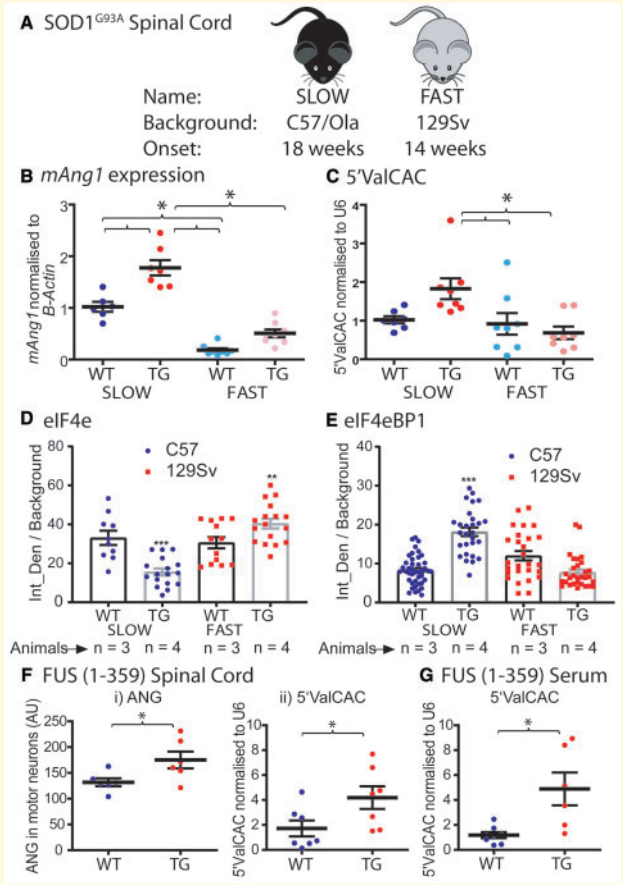

Figure 4 5′ValCAC tiRNA is elevated in a slow compared to a fast-progressing *SOD1*^{G93A} mouse model and in the spinal cord and serum from the FUS (1-359) mouse model. (**A**) Cartoon showing differences in disease progression between SLOW (C57Bl/6JOlaHsd) and FAST (Sv129) mice carrying the *SOD1*^{G93A} transgene. (**B**) *mAng1* levels were analysed by qPCR in the lumbar spinal cord from WT and TG, SLOW and FAST mice carrying the *SOD1*^{G93A} transgene, confirming significantly elevated *mAng1* levels at symptom onset in spinal cord from slow progressing TG ALS mice. (**C**) 5′ValCAC tiRNA levels were significantly higher in TG mice on the slow progressing background. $N = 8$ mice per group, ANOVA with *post hoc* Tukey's for 5′ValCAC $P = 0.0079$, * indicates $P < 0.05$. Levels of protein translation initiation factors (**D**) eIF4e and (**E**) eIF4eBP1 were profiled in motor neurons by immunohistochemistry and quantified in relation to WT. Data are shown as mean ± SEM of the number of individual motor neurons analysed from three/four mice per group (animal numbers indicated below). Two-way ANOVA with *post hoc* Sidak was performed on the average Int_Den value for each mouse. $^{**}P < 0.01$; $^{***}P < 0.01$; $^{****}P < 0.0001$. (**D**) eIF4e was significantly decreased in TG mice from the SLOW colony and significantly increased in TG mice from the FAST colony indicating lower levels of eIF4e are beneficial to ALS disease progression. Representative images are shown in Supplementary Fig. 15. (**E**) Conversely, eIF4EBP1 was significantly elevated in TG mice from the SLOW colony and slightly lowered in TG mice from the FAST colony. Representative images are shown in Supplementary Fig. 15. F) In a second preclinical ALS mouse model the FUS (1-359) colony both (i) ANG and (ii) 5′ValCAC were significantly elevated in lumbar spinal cord from TG mice compared to WT littermates around symptom onset. ANG levels were quantified by immunohistochemistry in 6 WT and 6 TG mice per group, with representative images provided in Supplementary Fig. 17. G) 5′ValCAC was significantly elevated in serum collected at symptom onset from TG mice compared to WT littermates. For FUS (1-359) tissue samples $n = 7$ mice per group, for serum samples $n = 6$–8. * indicates significance of $P < 0.05$, two-tailed *t*-test. Individual data points are plotted with mean ± SEM, and significance indicated.

eIF4e is the rate-limiting factor in the protein translation process, and levels are tightly regulated via interaction with the eIF4e-BP inhibitor proteins, where eIF4e and eIF4e-BP1 are normally present in a 1:1 ratio (Rau *et al.*, 1996). Interestingly, 5′Alanine tiRNA has been shown to interact directly with eiF4e and can displace eIF4e from the 5′m7G cap (Ivanov *et al.*, 2011). To determine whether increased 5′ValCAC levels were associated with dysregulation of protein translation initiation factors, we examined the expression of eIF4e and eIF4eBP1 in motor neurons by immunohistochemistry. This revealed that slow-progressing TG mice had significantly lower levels of eIF4e and higher levels of eiF4eBP1 compared to WT mice on the same background (Fig. 4D and E and Supplementary Figs 15 and 16). The opposite was observed in the fast-progressing mice where eiF4e was significantly elevated in TG compared to WT mice, while eiF4eBP1 showed no significant difference but levels were lower in TG mice. Together, we observe an upregulation of Ang in motor neurons, along with increased 5′ValCAC levels in spinal cord homogenate, and altered levels of protein translation factors within motor neurons. It remains to be seen whether these changes occur as part of a synchronized stress response.

To determine whether 5′ValCAC levels were altered in a second ALS model, we employed the FUS (1-359) mouse model (Shelkovnikova *et al.*, 2013) from which spinal cord tissue and serum samples were available. FUS (1-359) TG mice overexpress a truncated human FUS gene lacking a nuclear localization signal, which is prone to cytoplasmic aggregation, and show an early vasculature defect similar to the SOD1^{G93A} model (Crivello *et al.*, 2018, 2019). We analysed mice collected at postnatal day 90 which equates to around symptom onset as the average lifespan of TG mice from the FUS (1-359) colony is 120 days (±22 days)(Hogg *et al.*, 2017). Immunohistochemistry of Ang protein (ANG) levels in lumbar motor neurons from 6 WT and 6 TG mice showed that ANG levels were significantly higher in TG mice than WT littermates (Fig. 4F (i) and Supplementary Fig. 17). Quantification of 5′ValCAC levels in lumbar spinal cord homogenate revealed that 5′ValCAC was significantly elevated in TG mice compared to WT littermates (Fig. 4F(ii)). As we have demonstrated that 5′ValCAC is secreted from cells, we sought to determine whether it could be detected in serum. We found that 5′ValCAC was significantly elevated in serum from TG FUS (1-359) mice compared to WT littermates at disease onset (Fig. 4G) indicating 5′ValCAC may be of use as a

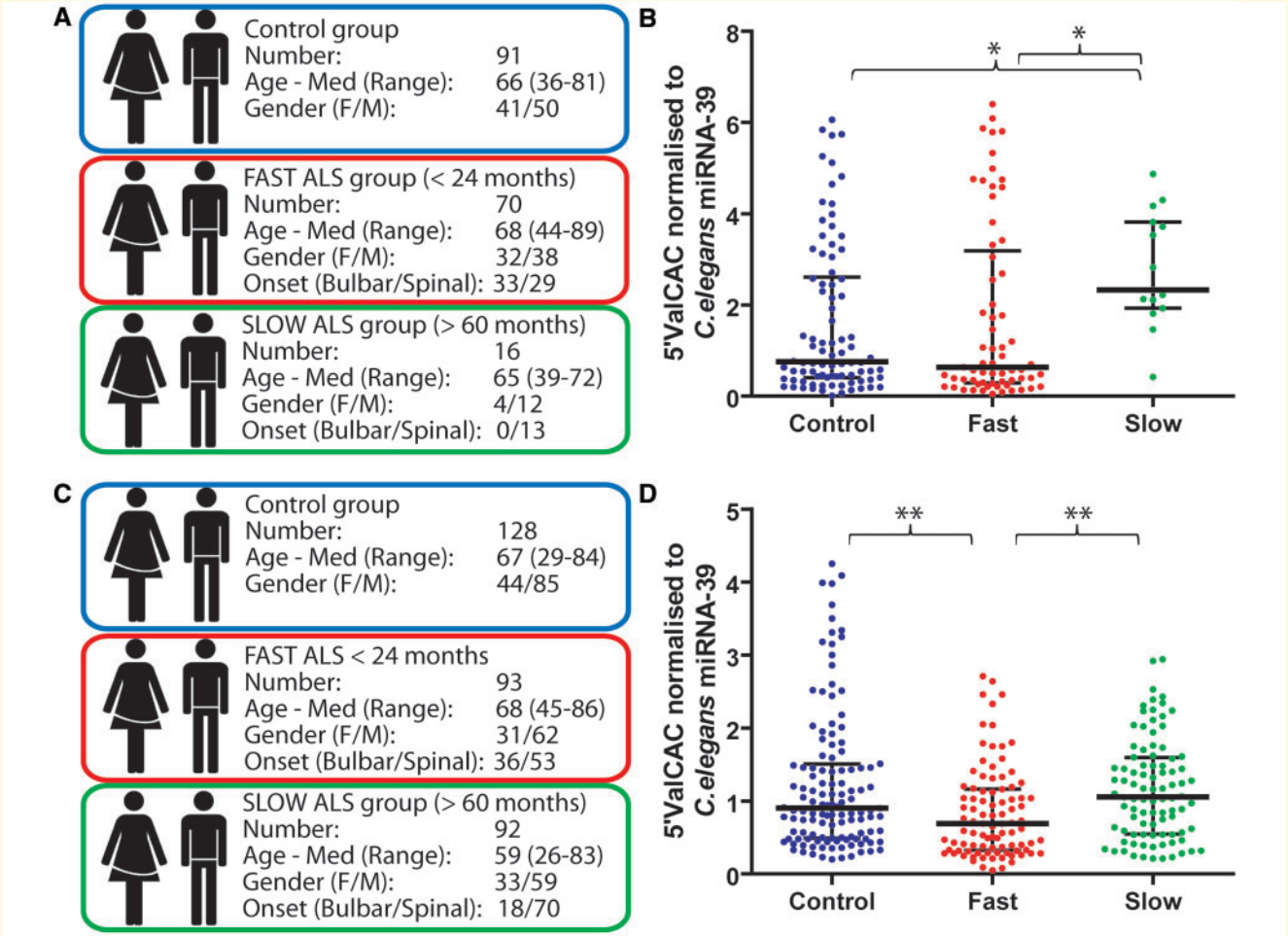

Figure 5 Serum 5′ValCAC levels are significantly elevated in ALS patients with slow progressing disease. Serum from a cohort of 114 ALS patients and 91 age and sex matched healthy controls from the Netherlands was investigated for tiRNA levels. (**A**) Demographics of human samples used and patient stratification based on survival to death or tracheostomy. (**B**) When patients were stratified by survival serum 5′ValCAC levels were significantly elevated in patients with slow progressing disease, both when compared to healthy controls and when compared to patients with fast-progressing disease (Kruskal–Wallis test $P = 0.012$, Dunn's *post hoc* test, $P < 0.05$ for fast versus slow and control versus slow. (**C**) Demographics of the validation cohort of ALS patients and healthy controls from the Netherlands. (**D**) A significant difference in serum 5′ValCAC levels between fast and slow progressing patients was confirmed in a second independent cohort of patients (Kruskal–Wallis test $P = 0.0005$, Dunn's *post hoc* test indicates $P < 0.01$ for fast versus slow and control versus fast). Individual data points are plotted with median and interquartile range indicated.

blood-based biomarker in ALS. Analysis of 5′ValCAC levels at a pre-symptomatic time point (post-natal day 50) revealed there was no significant difference in 5′ValCAC levels between WT and TG littermates in spinal cord or serum (Supplementary Fig. 18).

Serum 5′ValCAC levels as a prognostic biomarker for ALS patients

The preclinical data in the slow- and fast-progressing $SOD1^{G93A}$ TG mouse models suggested that 5′ValCAC levels are related to activation of protective stress responses during disease progression and may hold prognostic potential. To further explore the role of serum 5′ValCAC as a biomarker for ALS progression, we next investigated serum collected at diagnosis from a cohort of slow- and fast-progressing ALS patients ($n = 114$, consisting of $n = 70$ fast and $n = 16$ slow-progressing ALS patient) and 91 healthy controls in The Netherlands as part of the PAN Study (Huisman *et al.*, 2011). Patients were stratified according to disease progression determined by survival time: fast progressors <24 months and slow progressors >60 months (Fig. 5A). 5′ValCAC levels were significantly elevated in slow-progressing patients when compared to healthy controls or to fast-progressing patients indicating 5′ValCAC levels in serum may be of use as a prognostic biomarker in ALS (Fig. 5B: Kruskal–

Wallis test $P = 0.012$, Dunn's *post hoc* $P < 0.05$ for fast versus slow and control versus slow).

No significant correlation was found between 5′ValCAC levels and RNA concentration (Supplementary Fig. 19), and no significant difference was detected in 5′ValCAC levels from haemolysed and non-haemolysed samples (data not shown). ALS patients were screened for repeat expansions at the *C9orf72* locus, and whole exome sequencing was performed to screen for mutations at the *SOD1*, *TARDBP*, *FUS* and *ANG* loci (Supplementary Table 3). No significant difference was detected in 5′ValCAC levels in ALS patients with *C9orf72* repeat expansion compared to those without (wt), and no differences were detected in patients with *FUS*, *TARDBP* or *SOD1* mutations [Supplementary Fig. 20; $n = 4$, 2 and 3 respectively, labelled wt(+mut)]. Unfortunately, no patients in the discovery cohort carried mutations in *ANG*. These results suggest serum 5′ValCAC levels may provide prognostic information for sporadic and familial ALS patients, irrespective of whether an underlying genetic cause has been identified.

Next, findings were validated in a second independent cohort of serum samples from the PAN study (Huisman *et al.*, 2011). Serum samples collected at diagnosis from slow ($n = 92$) and fast ($n = 93$) progressing ALS patients and healthy controls ($n = 128$) were included to replicate the initial study and optimize contrast and power. Validation cohort demographics are shown (Fig. 5C). Analysis of serum 5′ValCAC levels indicated a significant difference across survival groups (Fig. 5D; Kruskal–Wallis test $P = 0.0005$, Dunn's *post hoc* $P < 0.01$ for control versus fast and fast versus slow). In unadjusted analyses, 5′ValCAC was significantly associated with disease progression when comparing controls, fast and slow ALS progressors ($P = 0.008$). For every unit increase in 5′ValCAC, the risk of slow versus fast ALS progression increased by 38% (relative risk 1.38, 95% confidence interval 1.01–1.89) and the risk of fast ALS progression versus controls decreased by 34% (relative risk 0.66, 95% confidence interval 0.49–0.89). Relative risk estimates and 95% confidence intervals were similar after adjusting for age and sex. Results were statistically significant after correcting for multiple comparisons (Bonferroni $P = 0.02$).

To determine whether serum 5′ValCAC levels could be prognostic for a continuous clinical spectrum of ALS patients, we combined cohorts 1 and 2 and additionally included an intermediate survival group from cohort 1 ($n = 16$) and cohort 2 ($n = 91$). To determine a cut-off value, we performed receiver operating characteristic curve analysis on fast and slow progressing patients from cohorts 1 and 2. This analysis gave an area under the curve of 0.66, with $P = 0.000003$ (Supplementary Fig. 21). Youden's J statistic indicated a cut-off value of 0.735 provided the best discrimination between fast and slow progressing patients, with a sensitivity of 82.9% and a specificity of 47.4%. We used this cut-off to stratify patients into low 5′ValCAC (<0.735) and high 5′ValCAC (>0.735) groups. Kaplan–Meier analysis of survival for high and low 5′ValCAC groups indicated that patients with high serum 5′ValCAC at diagnosis survived significantly longer than those with low 5′ValCAC levels (Fig. 6A; Log Rank test, $\chi^2 = 12.29$, $P = 0.0005$). The number of patients surviving at each 12-month time point is indicated below the x-axis (Fig. 6B). Of note, the prognostic value of 5′ValCAC levels remain when patients with the spinal-onset disease are analysed alone (Supplementary Fig. 22, Log-Rank test, $P = 0.008$), indicating that although spinal onset indicates a better prognosis, 5′ValCAC levels provide additional prognostic value. These data suggest 5′ValCAC levels in serum, collected at diagnosis, may provide prognostic information for ALS patients.

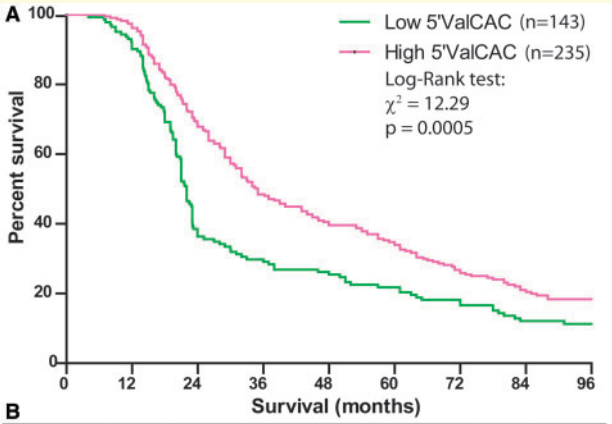

B

Months:	12	24	36	48	60	72	84	96
High	229	159	114	92	79	59	42	26
Low	132	53	41	36	31	24	17	13

Figure 6 Kaplan–Meier survival analysis indicates high 5′ValCAC at diagnosis holds prognostic value for a continuous spectrum of ALS patients. (**A**) ALS patients from cohorts 1 and 2 combined including intermediate survival group from cohort 2 ($n = 378$) were stratified into high and low 5′ValCAC groups using the cut-off 0.735. Kaplan–Meier survival analysis indicates patients with high 5′ValCAC survive for significantly longer than this with low 5′ValCAC levels, Log Rank test $\chi^2 = 12.29$, $P = 0.0005$. The median survival for the low 5′ValCAC group is 22 months and for the high 5′ValCAC is 35 months. (**B**) Patient survival numbers for each 12-month time point are indicated.

Discussion

Ang shows neuroprotective properties *in vitro* and loss of functional Ang due to mutation or decreased expression has been implicated in a range of neurodegenerative disorders (Greenway *et al.*, 2006; Kieran *et al.*, 2008; van Es *et al.*, 2011; Skorupa *et al.*, 2012; Gagliardi *et al.*, 2018). We sought to characterize Ang-generated tRNA fragments and investigated their prevalence throughout

disease progression in ALS. We found Ang cleaves a subset of tRNAs, and only one half is preserved. The tRNA fragments are predicted to form hairpin structures, which appear to be protected from degradation. Interestingly, we find that the 5′ValCAC fragment is significantly elevated in ALS mouse models and serum from ALS patients with a slow disease progression. The clinical findings were validated in the second cohort of ALS patients, suggesting that 5′ValCAC could serve as a novel prognostic biomarker.

Cleavage of tRNAs by Ang has been widely reported yet we were surprised as only a small subset of tRNAs were cleaved robustly (Fu *et al.*, 2009; Yamasaki *et al.*, 2009; Saikia *et al.*, 2012). We identified both 5′tiRNA and 3′tiRNAs in our screen yet never both from the same tRNA. Recent work has shown that tRNA cleavage by Ang can be inhibited by 5-methylcytosine indicating some tRNAs may be protected by the presence of RNA modifications (Schaefer *et al.*, 2010; Blanco *et al.*, 2014). Many reports describe the presence of tiRNA fragments in a range of cell types, animal models and human patients, but little is known about their function. They were originally described to inhibit protein translation (Yamasaki *et al.*, 2009; Ivanov *et al.*, 2011), promote stress granule assembly (Emara *et al.*, 2010) and were found to be neuroprotective in motor neurons (Ivanov *et al.*, 2014). More recently, several groups have reported that tRNA fragments can inhibit protein translation and regulate ribosome biogenesis (Kim *et al.*, 2017; Guzzi *et al.*, 2018; Fricker *et al.*, 2019). Translation initiation factor eIF4e plays a crucial role in recruiting the ribosome to the mRNA to initiate protein translation via binding to the 5′m7G cap structure. eIF4e interacts with scaffolding protein eIF4G which recruits the RNA helicase eIF4A to form the eIF4F complex. The eIF4F complex then engages with other initiation factors and ultimately recruits the large and small ribosomal subunits to allow protein translation to occur. eIF4e is the rate-limiting factor in the translation initiation process, and as such levels are tightly regulated under normal physiological conditions via interaction with eIF4eBP inhibitor proteins. Indeed, eIF4e and eIF4eBP1 are normally present in a 1:1 ratio (Rau *et al.*, 1996). Lower levels of eIF4e coupled with increased levels of eIF4eBP1 that we observed in TG mice from the slow-progressing $SOD1^{G93A}$ colony would likely result in decreased protein translation; however, translation initiation factors are also regulated via phosphorylation. Ivanov *et al.* (2011) demonstrated that 5′Alanine tiRNA can displace eIF4G from the m7G cap, and to a lesser extent eIF4e. Interestingly, when they analysed the proteins bound to 5′Alanine tiRNA they found that eIF4e precipitated at much higher levels than eiF4G. These data and our results suggest that tiRNAs may interact directly with eIF4e and influence cap-dependent protein translation; however, further work is required to determine whether these observations are linked. Of note, pharmacological intervention targeting protein translation with Guanabenz, which blocks dephosphorylation of translation initiation factor eIF2α, have been shown to improve motor performance, protect against motor neuron loss and extend lifespan in the $SOD1^{G93A}$ ALS mouse model (Jiang *et al.*, 2014; Wang *et al.*, 2014). However, a subsequent study found that Guanabenz exacerbated disease in $SOD1^{G93A}$ mice (Vieira *et al.*, 2015). Recently, Ang has been shown to preserve stemness in haematopoietic stem cells via the generation of tiRNAs that inhibit protein translation, whilst promoting the proliferation of myeloid progenitor cells via stimulation of ribosomal RNA (Goncalves *et al.*, 2016).

To date, little research has focused on the extracellular function of tRNA fragments, yet here we find 5′ValCAC to be secreted from neuronally derived cells. We found basal levels of 5′ValCAC within EVs secreted from neural cells overexpressing WT or mutant *Ang*, but higher levels of 5′ValCAC were found in the total CM fraction, indicating the majority of 5′ValCAC is secreted via a different pathway. Further, the un-encapsulated fraction of secreted 5′ValCAC was greatly influenced by mutations in *Ang* suggesting Ang may interact with the (as yet unidentified) factors involved in this pathway, within the cytoplasm. This is supported by the increased level of 5′Val CAC secretion we observed from cells overexpressing the R31K *Ang* mutant. Interestingly, sorting of RNAs, including tRNAs, prior to secretion in EVs can be dependent on the RNA sequence and the cell or tissue of origin, and YBX-1 protein has been implicated (Shurtleff *et al.*, 2017; Temoche-Diaz *et al.*, 2019). Un-encapsulated extracellular miRNAs have been found in complexes with high-density lipoproteins (Vickers *et al.*, 2011), nucleophosmins (Wang *et al.*, 2010) and argonaute protein complexes (Kumar *et al.*, 2014), indicating there are many potential candidates that may be involved in transporting un-encapsulated tiRNAs. Research on miRNAs has shown cell-type specific secretion and uptake occurs (Chivet *et al.*, 2014). This raises the possibility that extracellular tiRNAs may function similarly as specific signalling molecules, particularly within the CNS (Hogg *et al.*, 2019). tiRNAs have been shown to be generated in endothelial cells in response to hypoxia (Li *et al.*, 2016), and in airway epithelial cells in response to respiratory syncytial viral infection (Wang *et al.*, 2013), indicating that tiRNAs from sources other than spinal cord motor neurons may also contribute to tiRNAs quantified in serum in this study. Further investigations are required to determine how tiRNAs are secreted from neural cells and protected from degradation in circulation.

Serum Ang protein levels have been investigated as a biomarker of ALS and found to be elevated in ALS patients compared to controls (Cronin *et al.*, 2006; van Es *et al.*, 2014). Interestingly, in both studies serum Ang levels were higher in patients with spinal-onset ALS than those with bulbar onset, highlighting the role of Ang in spinal motor neurons under stress conditions. However,

there was no association between Ang levels and survival. This apparent discrepancy with our results can be explained as the levels of Ang protein were quantified in serum, whereas we postulate tRNA cleavage occurs within cells in the spinal cord, and the resulting tRNA fragments are secreted. Therefore, we posit that we are quantifying tRNA fragments as a measure of Ang activity within cells, as a 'read-out' of underlying stress response. As tiRNAs are widely reported to inhibit protein translation (Yamasaki *et al.*, 2009; Emara *et al.*, 2010; Ivanov *et al.*, 2011; Goncalves *et al.*, 2016) and have been shown to specifically inhibit cap-dependent translation (Ivanov *et al.*, 2011), they may alleviate neuronal stress by reducing cap-dependent translation while allowing vital stress-response factors to be generated via IRES-mediated translation.

There is a great need to develop prognostic biomarkers for ALS to monitor disease progression and treatment response and enable stratification of patients entering clinical trials. Here, we found that 5′ValCAC tiRNA levels are associated with a slower disease progression in both $SOD1^{G93A}$ ALS mouse model and ALS patient serum collected at diagnosis. tiRNAs generated by Ang occur as part of a highly conserved stress response, it is interesting to speculate that patients with a more robust stress response survive longer, although it cannot be excluded that these patients simply have a higher number of motor neurons surviving that are experiencing stress and exhibiting a stress response. Serum tiRNAs are highly suited for development as biomarkers as they are stable, serum is easily accessible, and the custom Taqman assays described here are reliable and easy to perform. Further, we have recently developed an electrochemical direct detection method for quantification of tRNA fragments in small volume biofluids which could be utilized for prognostic profiling of patients upon entry into clinical trials (McArdle *et al.*, 2020). Therefore, we present a novel class of non-coding RNA, which may be of use as a prognostic biomarker indicating a protective neuronal stress response in ALS patients. Further, our data suggest that the previously reported beneficial effects of Ang administered as a therapeutic in $SOD1^{G93A}$ mice may result from the 5′ValCAC tiRNA fragment. 5′ValCAC warrants further investigation in ALS to determine whether beneficial effects of Ang are mediated by this tRNA fragment.

Supplementary data

Supplementary material is available at *Brain Communications* online.

Acknowledgements

We would like to thank the patients who participated in this study.

Funding

This study was supported by grants awarded to J.H.M.P. from the Health Research Board (HRB_POR/2013/348), the Thierry Latran Foundation (FTL AP2011 PREHN), and from Science Foundation Ireland (17/JPND/3455 and SFI FutureNeuro Research Centre 16/RC/3948 co-funded under the European Regional Development Fund and by FutureNeuro industry partners). L.H.v.d.B. reports grants from Netherlands ALS Foundation, the Netherlands Organization for Health Research and Development (Vici scheme), and the Netherlands Organization for Health Research and Development (SOPHIA, STRENGTH, ALS-CarE project), funded through the EU Joint Programme–Neurodegenerative Disease Research, (JPND). M.A.v.E. received grants from the Netherlands Organization for Health Research and Development (Veni scheme), The Thierry Latran foundation and the Netherlands ALS foundation (Stichting ALS Nederland). C.B. reports grants from the 'Fondazione Regionale per la Ricerca Biomedica' (TRANS-ALS project). M.C.H. reports a grant from the ALS Association (20-IIP-513).

Competing interests

L.H.v.d.B. served on the Scientific Advisory Board of Biogen and Cytokinetics. M.A.v.E. received travel grants from Baxalta.The other authors report no competing interests.

References

Aparicio-Erriu IM, Prehn JH. Molecular mechanisms in amyotrophic lateral sclerosis: the role of angiogenin, a secreted RNase. Front Neurosci 2012; 6: 167.

Appierto V, Callari M, Cavadini E, Morelli D, Daidone MG, Tiberio P. A lipemia-independent NanoDrop((R))-based score to identify hemolysis in plasma and serum samples. Bioanalysis 2014; 6: 1215–26.

Blanco S, Dietmann S, Flores JV, Hussain S, Kutter C, Humphreys P, et al. Aberrant methylation of tRNAs links cellular stress to neurodevelopmental disorders. EMBO J 2014; 33: 2020–39.

Brooks BR. El Escorial World Federation of Neurology criteria for the diagnosis of amyotrophic lateral sclerosis. Subcommittee on Motor Neuron Diseases/Amyotrophic Lateral Sclerosis of the World Federation of Neurology Research Group on Neuromuscular Diseases and the El Escorial "Clinical limits of amyotrophic lateral sclerosis" workshop contributors. J Neurol Sci 1994; 124: 96–107.

Chakrabortty SK, Prakash A, Nechooshtan G, Hearn S, Gingeras TR. Extracellular vesicle-mediated transfer of processed and functional RNY5 RNA. RNA 2015; 21: 1966–79.

Chan PP, Lowe TM. GtRNAdb: a database of transfer RNA genes detected in genomic sequence. Nucleic Acids Res 2009; 37: D93–97.

Chen X, Liang H, Zhang J, Zen K, Zhang CY. Secreted microRNAs: a new form of intercellular communication. Trends Cell Biol 2012; 22: 125–32.

Chivet M, Javalet C, Laulagnier K, Blot B, Hemming FJ, Sadoul R. Exosomes secreted by cortical neurons upon glutamatergic synapse activation specifically interact with neurons. J Extracell Vesicles 2014; 3: 24722.

Crivello M, Hogg MC, Jirstrom E, Halang L, Woods I, Rayner M, et al. Vascular regression precedes motor neuron loss in the FUS (1-359) ALS mouse model. Dis Model Mech 2019; 12. doi: 10.1242/dmm.040238.

Crivello M, O'Riordan SL, Woods I, Cannon S, Halang L, Coughlan KS, et al. Pleiotropic activity of systemically delivered angiogenin in the SOD1(G93A) mouse model. Neuropharmacology 2018; 133: 503–11.

Cronin S, Greenway MJ, Ennis S, Kieran D, Green A, Prehn JH, et al. Elevated serum angiogenin levels in ALS. Neurology 2006; 67: 1833–6.

Dolzhenko E, van Vugt J, Shaw RJ, Bekritsky MA, van Blitterswijk M, Narzisi G, et al.; The US–Venezuela Collaborative Research Group. Detection of long repeat expansions from PCR-free whole-genome sequence data. Genome Res 2017; 27: 1895–903.

Emara MM, Ivanov P, Hickman T, Dawra N, Tisdale S, Kedersha N, et al. Angiogenin-induced tRNA-derived stress-induced RNAs promote stress-induced stress granule assembly. J Biol Chem 2010; 285: 10959–68.

Fricker R, Brogli R, Luidalepp H, Wyss L, Fasnacht M, Joss O, et al. A tRNA half modulates translation as stress response in *Trypanosoma brucei*. Nat Commun 2019; 10: 118.

Fu H, Feng J, Liu Q, Sun F, Tie Y, Zhu J, et al. Stress induces tRNA cleavage by angiogenin in mammalian cells. FEBS Lett 2009; 583: 437–42.

Gagliardi S, Davin A, Bini P, Sinforiani E, Poloni TE, Polito L, et al. A novel nonsense angiogenin mutation is associated with Alzheimer disease. Alzheimer Dis Assoc Disord 2019; 33: 163–165.

Goncalves KA, Silberstein L, Li S, Severe N, Hu MG, Yang H, et al. Angiogenin promotes hematopoietic regeneration by dichotomously regulating quiescence of stem and progenitor cells. Cell 2016; 166: 894–906.

Greenway MJ, Andersen PM, Russ C, Ennis S, Cashman S, Donaghy C, et al. ANG mutations segregate with familial and 'sporadic' amyotrophic lateral sclerosis. Nat Genet 2006; 38: 411–3.

Guzzi N, Cieśla M, Ngoc PCT, Lang S, Arora S, Dimitriou M, et al. Pseudouridylation of tRNA-derived fragments steers translational control in stem cells. Cell 2018; 173: 1204–16.

Hetschko H, Voss V, Seifert V, Prehn JH, Kogel D. Upregulation of DR5 by proteasome inhibitors potently sensitizes glioma cells to TRAIL-induced apoptosis. FEBS J 2008; 275: 1925–36.

Hogg MC, Halang L, Woods I, Coughlan KS, Prehn JHM. Riluzole does not improve lifespan or motor function in three ALS mouse models. Amyotroph Lateral Scler Frontotemporal Degener 2018; 19: 438–45.

Hogg MC, Raoof R, El Naggar H, Monsefi N, Delanty N, O'Brien DF, et al. Elevation in plasma tRNA fragments precede seizures in human epilepsy. J Clin Invest 2019; 130. doi: 10.1172/JCI126346.

Honda S, Kirino Y. SHOT-RNAs: a novel class of tRNA-derived functional RNAs expressed in hormone-dependent cancers. Mol Cell Oncol 2016; 3: e1079672.

Huisman MH, de Jong SW, van Doormaal PT, Weinreich SS, Schelhaas HJ, van der Kooi AJ, et al. Population based epidemiology of amyotrophic lateral sclerosis using capture-recapture methodology. J Neurol Neurosurg Psychiatry 2011; 82: 1165–70.

Ivanov P, Emara MM, Villen J, Gygi SP, Anderson P. Angiogenin-induced tRNA fragments inhibit translation initiation. Mol Cell 2011; 43: 613–23.

Ivanov P, O'Day E, Emara MM, Wagner G, Lieberman J, Anderson P. G-quadruplex structures contribute to the neuroprotective effects of angiogenin-induced tRNA fragments. Proc Natl Acad Sci USA 2014; 111: 18201–6.

Jiang HQ, Ren M, Jiang HZ, Wang J, Zhang J, Yin X, et al. Guanabenz delays the onset of disease symptoms, extends lifespan, improves motor performance and attenuates motor neuron loss in the SOD1 G93A mouse model of amyotrophic lateral sclerosis. Neuroscience 2014; 277: 132–8.

Kieran D, Sebastia J, Greenway MJ, King MA, Connaughton D, Concannon CG, et al. Control of motoneuron survival by angiogenin. J Neurosci 2008; 28: 14056–61.

Kim HK, Fuchs G, Wang S, Wei W, Zhang Y, Park H, et al. A transfer-RNA-derived small RNA regulates ribosome biogenesis. Nature 2017; 552: 57–62.

Kim SW, Li Z, Moore PS, Monaghan AP, Chang Y, Nichols M, et al. A sensitive non-radioactive northern blot method to detect small RNAs. Nucleic Acids Res 2010; 38: e98–e98.doi: 10.1093/nar/gkp1235.

Kumar P, Anaya J, Mudunuri SB, Dutta A. Meta-analysis of tRNA derived RNA fragments reveals that they are evolutionarily conserved and associate with AGO proteins to recognize specific RNA targets. BMC Biol 2014; 12: 78.

Lee SR, Collins K. Starvation-induced cleavage of the tRNA anticodon loop in Tetrahymena thermophila. J Biol Chem 2005; 280: 42744–9.

Li H, Wu C, Aramayo R, Sachs MS, Harlow ML. Synaptic vesicles contain small ribonucleic acids (sRNAs) including transfer RNA fragments (trfRNA) and microRNAs (miRNA). Sci Rep 2015; 5: 14918.

Li Q, Hu B, Hu GW, Chen CY, Niu X, Liu J, et al. tRNA-derived small non-coding RNAs in response to. Sci Rep 2016; 6: 20850.

Livak KJ, Schmittgen TD. Analysis of relative gene expression data using real-time quantitative PCR and the 2(-Delta Delta C(T)) method. Methods 2001; 25: 402–8.

Lorenz R, Bernhart SH, Honer Zu Siederdissen C, Tafer H, Flamm C, Stadler PF, et al. ViennaRNA Package 2.0. Algorithms Mol Biol 2011; 6: 26.

Love MI, Huber W, Anders S. Moderated estimation of fold change and dispersion for RNA-seq data with DESeq2. Genome Biol 2014; 15: 550.

McArdle H, Hogg MC, Bauer S, Rosenow F, Prehn JHM, Adamson K, et al. Quantification of tRNA fragments by electrochemical direct detection in small volume biofluid samples. Sci Rep 2020; 10: 7516.

Nardo G, Iennaco R, Fusi N, Heath PR, Marino M, Trolese MC, et al. Transcriptomic indices of fast and slow disease progression in two mouse models of amyotrophic lateral sclerosis. Brain 2013; 136: 3305–32.

Pupillo E, Messina P, Logroscino G, Beghi E; the SLALOM Group. Long-term survival in amyotrophic lateral sclerosis: a population-based study. Ann Neurol 2014; 75: 287–97.

Raponi E, Agenes F, Delphin C, Assard N, Baudier J, Legraverend C, et al. S100B expression defines a state in which GFAP-expressing cells lose their neural stem cell potential and acquire a more mature developmental stage. Glia 2007; 55: 165–77.

Rau M, Ohlmann T, Morley SJ, Pain VM. A reevaluation of the cap-binding protein, eIF4E, as a rate-limiting factor for initiation of translation in reticulocyte lysate. J Biol Chem 1996; 271: 8983–90.

Saikia M, Jobava R, Parisien M, Putnam A, Krokowski D, Gao XH, et al. Angiogenin-cleaved tRNA halves interact with cytochrome C, protecting cells from apoptosis during osmotic stress. Mol Cell Biol 2014; 34: 2450–63.

Saikia M, Krokowski D, Guan BJ, Ivanov P, Parisien M, Hu GF, et al. Genome-wide identification and quantitative analysis of cleaved tRNA fragments induced by cellular stress. J Biol Chem 2012; 287: 42708–25.

Schaefer M, Pollex T, Hanna K, Tuorto F, Meusburger M, Helm M, et al. RNA methylation by Dnmt2 protects transfer RNAs against stress-induced cleavage. Genes Dev 2010; 24: 1590–5.

Sebastia J, Kieran D, Breen B, King MA, Netteland DF, Joyce D, et al. Angiogenin protects motoneurons against hypoxic injury. Cell Death Differ 2009; 16: 1238–47.

Shapiro R, Riordan JF, Vallee BL. Characteristic ribonucleolytic activity of human angiogenin. Biochemistry 1986; 25: 3527–32.

Shelkovnikova TA, Peters OM, Deykin AV, Connor-Robson N, Robinson H, Ustyugov AA, et al. Fused in sarcoma (FUS) protein lacking nuclear localization signal (NLS) and major RNA binding

motifs triggers proteinopathy and severe motor phenotype in transgenic mice. J Biol Chem 2013; 288: 25266–74.

Shurtleff MJ, Yao J, Qin Y, Nottingham RM, Temoche-Diaz MM, Schekman R, et al. Broad role for YBX1 in defining the small noncoding RNA composition of exosomes. Proc Natl Acad Sci USA 2017; 114: E8987–E8995.

Skorupa A, King MA, Aparicio IM, Dussmann H, Coughlan K, Breen B, et al. Motoneurons secrete angiogenin to induce RNA cleavage in astroglia. J Neurosci 2012; 32: 5024–38.

Steidinger TU, Standaert DG, Yacoubian TA. A neuroprotective role for angiogenin in models of Parkinson's disease. J Neurochem 2011; 116: 334–41.

Suzuki K, Bose P, Leong-Quong RY, Fujita DJ, Riabowol K. REAP: a two minute cell fractionation method. BMC Res Notes 2010; 3: 294.

Temoche-Diaz MM, Shurtleff MJ, Nottingham RM, Yao J, Fadadu RP, Lambowitz AM, et al. Distinct mechanisms of microRNA sorting into cancer cell-derived extracellular vesicle subtypes. Elife 2019; 8. doi: 10.7554/eLife.47544.

Thiyagarajan N, Ferguson R, Subramanian V, Acharya KR. Structural and molecular insights into the mechanism of action of human angiogenin-ALS variants in neurons. Nat Commun 2012; 3: 1121.

van Es MA, Hardiman O, Chio A, Al-Chalabi A, Pasterkamp RJ, Veldink JH, et al. Amyotrophic lateral sclerosis. Lancet 2017; 390: 2084–98.

van Es MA, Schelhaas HJ, van Vught PW, Ticozzi N, Andersen PM, Groen EJ, et al. Angiogenin variants in Parkinson disease and amyotrophic lateral sclerosis. Ann Neurol 2011; 70: 964–73.

van Es MA, Veldink JH, Schelhaas HJ, Bloem BR, Sodaar P, van Nuenen BF, et al. Serum angiogenin levels are elevated in ALS, but not Parkinson's disease. J Neurol Neurosurg Psychiatry 2014; 85: 1439–40.

van Rheenen W, Shatunov A, Dekker AM, McLaughlin RL, Diekstra FP, Pulit SL et al.; PARALS Registry. Genome-wide association analyses identify new risk variants and the genetic architecture of amyotrophic lateral sclerosis. Nat Genet 2016; 48: 1043–8.

Vickers KC, Palmisano BT, Shoucri BM, Shamburek RD, Remaley AT. MicroRNAs are transported in plasma and delivered to recipient cells by high-density lipoproteins. Nat Cell Biol 2011; 13: 423–33.

Vieira FG, Ping Q, Moreno AJ, Kidd JD, Thompson K, Jiang B, et al. Guanabenz treatment accelerates disease in a mutant SOD1 mouse model of ALS. PLoS One 2015; 10: e0135570.

Wang K, Zhang S, Weber J, Baxter D, Galas DJ. Export of microRNAs and microRNA-protective protein by mammalian cells. Nucleic Acids Res 2010; 38: 7248–59.

Wang L, Popko B, Tixier E, Roos RP. Guanabenz, which enhances the unfolded protein response, ameliorates mutant SOD1-induced amyotrophic lateral sclerosis. Neurobiol Dis 2014; 71: 317–24.

Wang Q, Lee I, Ren J, Ajay SS, Lee YS, Bao X. Identification and functional characterization of tRNA-derived RNA fragments (tRFs) in respiratory syncytial virus infection. Mol Ther 2013; 21: 368–79.

Wu D, Yu W, Kishikawa H, Folkerth RD, Iafrate AJ, Shen Y, et al. Angiogenin loss-of-function mutations in amyotrophic lateral sclerosis. Ann Neurol 2007; 62: 609–17.

Yamasaki S, Ivanov P, Hu GF, Anderson P. Angiogenin cleaves tRNA and promotes stress-induced translational repression. J Cell Biol 2009; 185: 35–42.